HIV protease inhibitors provide neuroprotection through inhibition of mitochondrial apoptosis in mice

Toshio Hisatomi,[1,2] Toru Nakazawa,[1] Kousuke Noda,[1] Lama Almulki,[1] Shinsuke Miyahara,[1] Shintaro Nakao,[1,2] Yasuhiro Ito,[1] Haicheng She,[1] Riichiro Kohno,[2] Norman Michaud,[1] Tatsuro Ishibashi,[2] Ali Hafezi-Moghadam,[1] Andrew D. Badley,[3] Guido Kroemer,[4,5,6] and Joan W. Miller[1]

[1]Angiogenesis Laboratory, Massachusetts Eye and Ear Infirmary, Harvard Medical School, Boston, Massachusetts, USA. [2]Department of Ophthalmology, Graduate School of Medical Sciences, Kyushu University, Fukuoka, Japan. [3]Division of Infectious Diseases, Mayo Clinic, Rochester, Minnesota, USA. [4]INSERM, U848, Villejuif, France. [5]Institut Gustave Roussy, Villejuif, France. [6]Université Paris-Sud 11, Villejuif, France.

Neuroprotection can be achieved by preventing apoptotic death of postmitotic cells. Apoptotic death can occur by either a caspase-dependent mechanism, involving cytochrome *c*, apoptosis protease-activating factor–1 (Apaf-1), and caspase-9, or a caspase-independent mechanism, involving apoptosis-inducing factor (AIF). HIV protease inhibitors (PIs) avert apoptosis in part by preventing mitochondrial outer membrane permeabilization (MOMP), but the precise mechanism by which they work is not known. Here, we evaluated the impact of the PIs in a mouse model of retinal detachment (RD) in vivo and in murine primary retinal cell cultures in vitro. Oral administration of the PIs nelfinavir and ritonavir significantly inhibited photoreceptor apoptosis, while preventing the translocation of AIF from mitochondria to the nucleus as well as the activation of caspase-9. RD-induced photoreceptor apoptosis was similarly inhibited in mice carrying hypomorphic mutations of the genes encoding AIF or Apaf-1. Nelfinavir attenuated apoptosis as well as mitochondrial release of AIF and cytochrome *c*, and subsequent activation of caspase-9 in vitro, in photoreceptor cultures exposed to starvation or monocyte chemoattractant protein–1–stimulated (MCP-1–stimulated) macrophages. Our results suggest that the MOMP inhibition by PIs involved interruption of both caspase-dependent and caspase-independent apoptosis pathways and that PIs may be clinically useful for the treatment of diseases caused by excessive apoptosis.

Introduction

Photoreceptor apoptosis after retinal detachment (RD) is a major cause of permanent visual loss in various diseases. Detachment of the retina from underlying retinal pigment epithelium (RPE) occurs in a variety of ocular disorders, including age-related macular degeneration (AMD) (1), diabetic retinopathy (2), retinopathy of prematurity (3), as well as rhegmatogenous, tractional, and exudative RD (4, 5).

Although surgery can reattach the retina, visual acuity is not always restored due to photoreceptor apoptosis during RD (4–8). Recently, we reported that early inhibition of the infiltration of bone marrow–derived macrophage/microglia into the detached retina may prevent photoreceptor apoptosis in animal models (9, 10). However, in some patients, attempts at preventing macrophage/microglia activation may come late. Therefore, it is critical to identify downstream mediators of photoreceptor apoptosis following macrophage/microglia infiltration, for instance, during the intracellular signaling phase, to prevent visual loss after RD. Such insights may lead to new treatments for many important retinal disorders.

Most cell death in vertebrates proceeds via the mitochondrial pathway of apoptosis (11). Mitochondria contain proapoptotic factors such as cytochrome *c* and apoptosis-inducing factor (AIF) in their intermembrane space. Furthermore, mitochondrial outer membrane permeabilization (MOMP) is a critical event during apoptosis, representing the "point of no return" of the lethal process. Cytochrome *c* is released from mitochondria upon MOMP and binds to cytosolic apoptotic protease-activating factor–1 (Apaf-1) to induce its dimerization and a conformational change (12). Apaf-1 then oligomerizes into apoptosomes that recruit and activate caspase-9, followed by serial activation of apoptosis execution molecules (13, 14). However, MOMP may cause cell death even if caspases are inhibited (15), and a broad caspase inhibitor, Z-VAD-FMK, fails to block photoreceptor apoptosis in experimental RD (6). AIF is a caspase-independent apoptogenic factor and is normally confined to the mitochondrial intermembrane space (16). During apoptosis, AIF translocates to the cytosol and then to the nucleus, where it triggers peripheral chromatin condensation and interacts with cyclophilin A to generate a DNAse complex that is responsible for the so-called large-scale DNA degradation to fragments of approximately 50 kbp (16, 17). Since we originally reported AIF translocation in mammalian cells in vivo in a model of RD (6), the translocation of AIF has been reported in neurodegeneration (18, 19) and retinal degeneration (20). However, the contribution of AIF to RD-associated photoreceptor apoptosis has remained elusive. Furthermore, novel splice variants of AIF have

Nonstandard abbreviations used: AIF, apoptosis-inducing factor; Apaf-1, apoptotic protease-activating factor–1; MCP-1, monocyte chemoattractant protein–1; MOMP, mitochondrial outer membrane permeabilization; NFV, nelfinavir; ONL, outer nuclear layer; PI, protease inhibitor; RD, retinal detachment; RIT, ritonavir.

Conflict of interest: The authors have declared that no conflict of interest exists.

Citation for this article: *J. Clin. Invest.* **118**:2025–2038 (2008). doi:10.1172/JCI34267.

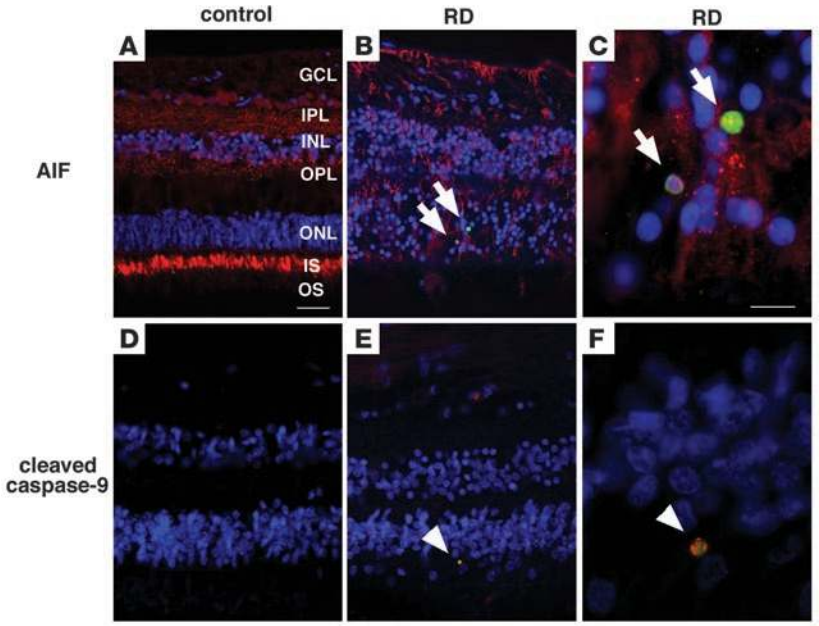

Figure 1
Immunofluorescence detection of AIF and cleaved caspase-9 in the human retina after RD. Paraffin-embedded retinal sections from the MEEI archives were analyzed retrospectively. Whereas histopathologic sections showed relatively preserved retinal structures in control retinas without RD (**A** and **D**), photoreceptor loss and secondary gliosis were observed in retinas with RD (**B**, **C**, **E**, and **F**). Specific AIF-staining was noted in ganglion cells (GCL), inner plexiform layer (IPL), inner nuclear layer (INL), outer plexiform layer (OPL), and photoreceptor inner segment (IS) and outer segment (OS) of control retina (**A**; AIF in red, TUNEL in green, DAPI in blue). Notably, in the detached retinas, AIF staining was mainly observed in proliferating glial cells as well as in TUNEL-positive photoreceptor nuclei (**B** and **C**, arrows). Although no staining was observed in control retinas without RD (**D**), cleaved caspase-9–positive cells were noted in the cytoplasm of TUNEL-positive cells in the detached retinas (cleaved caspase-9 in red, TUNEL in green, DAPI in blue; arrowheads in **E** and **F**). Scale bars: 50 μm (**A**, **B**, **D**, and **E**) and 10 μm (**C** and **F**).

been reported (21), and the role of AIFsh, a proapoptotic short variant that may be transcriptionally induced after apoptotic insults (22), remains largely unknown.

The death of postmitotic cells in the CNS and retina is the final result of acute or chronic degenerative processes and is a target for neuroprotection by inhibiting apoptotic signaling (23). HIV protease inhibitors (PIs) were originally designed to block the formation of HIV viral proteins by viral proteases and are currently administered to millions of patients with HIV worldwide (24). Recently, it has been reported that PIs not only inhibit virus replication but also suppress $CD4^+$ T lymphocyte apoptosis at concentrations similar to those that are achieved in the plasma of PI-treated patients (25). In several cases, HIV-infected individuals recovered normal levels of circulating $CD4^+$ T cells upon PI treatment, although the therapy had no effects on the viral titers, suggesting that PIs might inhibit apoptosis of $CD4^+$ T cells in vivo, independent of their effect on HIV replication (24, 26, 27). Several groups have investigated the mechanisms by which PIs inhibit apoptosis. Altered transcriptional regulation of regulatory proteins (28), as well as direct inhibition of caspase-1 (29) or calpain (30), have been reported. However, these proposed mechanisms may not explain the ability of PIs to block cell death induced by a wide range of apoptotic insults (25) and are not compatible with other studies reporting poor effects of PIs on effector caspases (31) or the net synthesis of apoptosis regulators (31). Recently, PIs were shown to inhibit the MOMP-dependent release of cytochrome *c* (31–33) via direct binding to and inhibition of the adenine nucleotide translocator, a protein from the inner mitochondrial membrane that can form pores and mediate MOMP (34). However the protective effects of PIs contrast with the observation that pharmacological caspase inhibitors largely fail to inhibit cell death (23). We hypothesized that PIs may simultaneously block caspase-dependent and caspase-independent cell death pathways, via blocking MOMP, and tested this possibility in a model of RD-induced photoreceptor degeneration.

The objectives of this study were, first, to investigate the mechanism of apoptotic signaling in the neurodegeneration model of RD and to evaluate the relative contribution of AIF and the cytochrome *c*/Apaf-1–driven caspase activation cascade. Second, we explored whether and through which mechanisms systemic oral administration of PIs would mediate antiapoptotic effects in RD. In this work, we demonstrate the HIV PIs inhibit the mitochondrial release of AIF and cytochrome *c*. Thus, HIV PIs interrupt both the caspase-dependent (cytochrome *c*/Apaf-1/caspase-9–mediated) and the caspase-independent (AIF-mediated) pathways of apoptotic self-destruction that originate in the mitochondria.

Results

AIF translocation and caspase activation in apoptotic photoreceptors in human and mouse retina after RD. Histopathological examination of detached retinas, as compared with control retinas, revealed disorganization of the strata, loss of photoreceptors, and secondary gliosis (Figure 1). Immunohistochemistry demonstrated specific AIF staining in ganglion cells, the inner plexiform, inner nuclear, and outer plexiform layers, as well as in photoreceptor inner segments from control retinas, in line with our previous observations in rats (6, 18) (Figure 1A). In the detached retinas, AIF staining was observed in proliferating glial cells as well as in TUNEL-positive apoptotic photoreceptor nuclei (Figure 1, B and C). While control retinas stained negatively with an antibody recognizing cleaved, active casapse-9 (Figure 1D), the cytoplasm of TUNEL-positive cells from detached retinas did exhibit a fluorescence signal indicative of the presence of active caspase-9 (Figure 1, E and F). These results indicate that both the activation of caspase and the mitochondrio-nuclear translocation of the caspase-independent death effector AIF occur in human retinas after RD. Similar results were obtained after experimental RD in mice, indicating a redistribution of AIF (Figure 2, A and B) and the activation of caspase-9 and -3 (Figure 2, C–F), following an overall pattern that was comparable to that in human RD. Exactly as in humans, after RD, murine retinas contained AIF within TUNEL-positive photoreceptor nuclei (Figure 2B) and activated caspases in the cytoplasm of apoptotic cells (Figure 2, D and F). These results indicate that the caspase-

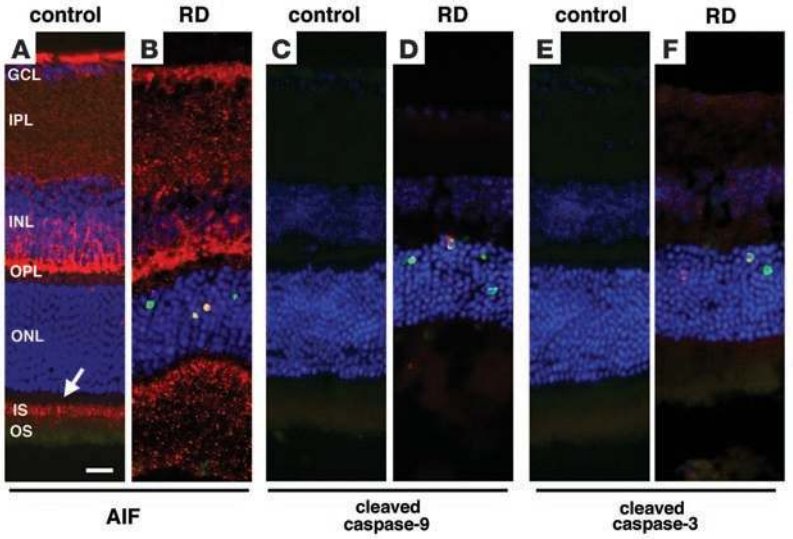

Figure 2
Immunofluorescence detection of AIF and cleaved caspase-9 and -3 in the mouse retina after RD. AIF-positive staining was noted in ganglion cells, inner plexiform layer, inner nuclear layer, outer plexiform layer, and photoreceptor inner segment (arrow) of control retinas (**A**; AIF in red, TUNEL in green, DAPI in blue). After RD, photoreceptors underwent apoptotic cell death, and AIF-positive staining was observed in TUNEL-positive photoreceptor nuclei (**B**). Cytosolic staining of cleaved caspase-9 (**D**, red) and -3 (**F**, red) was observed in the detached retinas but not in control attached retinas (**C** and **E**). Scale bar: 10 μm.

dependent and caspase-independent pathways follow a similar spatiotemporal activation pattern in humans and mice, suggesting that mouse RD constitutes an accurate model of human RD.

AIF deficiency protects from RD-induced photoreceptor apoptosis. Harlequin (*Hq*) mice exhibit an X chromosome–linked ataxia due to the progressive degeneration of terminally differentiated cerebellar neurons (35, 36). The *Hq* mutation has been identified as a proviral insertion in the *Aif* gene, also known as programmed cell death 8 (*Pdcd8*), causing about 80% reduction in AIF expression (36). In contrast to *Aif*-knockout mice (which die in utero) (37), *Hq* mice are born at normal Mendelian ratios and are healthy until the age of 3 months. We comparatively assessed the mRNA and protein expression of AIF and AIFsh, a proapoptotic short variant that is reported to be induced after apoptotic insults (22), by RT-PCR (Figure 3, A and B), immunoblotting (Figure 3C), or immunohistochemistry (Figure 3, D–I), in hemizygote (*Hq*/Y) and WT (+/Y) retinas. As compared with WT controls, *Hq*/Y retinas contained negligible levels (<10% of control values) of AIF mRNA or protein (Figure 3, A, C, D, E, G, and H). The AIFsh mRNA expression was also decreased in *Hq*/Y mice (Figure 3A), and AIFsh mRNA did not increase (and actually decreased) 3 days after RD (Figure 3B). No differences in retinal morphology were observed between *Hq*/Y and WT littermates before 3 months of age (36). However, *Hq*/Y mice manifested a gradual loss of the ganglion cell layer and the inner and outer nuclear layers (ONLs) after 4 months. Thus, the general appearance of the retina and the thickness of the ONL were similar in untreated 8-week-old *Hq*/Y and WT mice, that is, at the age at which experiments were performed (Figure 3, D and G). The frequency of photoreceptor apoptosis was slightly higher than that in WT mice under normal conditions (Figure 3J). However, after RD, *Hq*/Y retinas exhibited significantly less TUNEL-positive apoptotic cells than WT controls (Figure 3, E, H, and J) and exhibited reduced cell loss, as assessed by counting the number of cells in the ONL (Figure 3K) or measuring ONL thickness (Figure 3L). The remaining TUNEL-positive apoptotic photoreceptors showed activated, cleaved caspase-9 in *Hq*/Y mice (Figure 3, F and I). Transmission electron microscopy also revealed well-preserved rod spherules and cone pedicles in the outer plexiform layer (Figure 3, M and P, arrowheads), decreased apoptotic nuclei in the ONL (Figure 3, N and Q, arrows), and relatively well preserved mitochondria in the inner segment of photoreceptors (Figure 3, O and R, white arrows) from detached *Hq*/Y retinas, as compared with WT retinas. This the first evidence to our knowledge that AIF is involved in RD-induced photoreceptor degeneration.

Apaf-1 deficiency protects from RD-induced photoreceptor apoptosis. The "forebrain overgrowth" (*fog*) mutation leads to an autosomal recessive neural tube closure defect due to the near-complete lack of Apaf-1 expression (38, 39). However, a complete deficiency in *Apaf-1* usually results in perinatal lethality, while *fog/fog* mice more readily survive into adulthood (39, 40), allowing us to assess the role of Apaf-1 and Apaf-1–dependent cytochrome *c*–mediated caspase activation in photoreceptor apoptosis after RD. *Apaf-1*$^{-/-}$ embryos possess thicker retinas than normal littermates around E12.5–E14.5, due to a hyperplastic ganglion cell layer (41, 42). Adult, 8-week-old Apaf-1 mutant (*fog/fog*) and WT mice exhibited a similar histological appearance of the retina and ONL thickness (Figure 4, A and D) and a similar low frequency of apoptotic photoreceptors under normal conditions. Apaf-1 deficiency reduced the RD-induced photoreceptor apoptosis, as assessed by TUNEL staining (Figure 4, A–G), and simultaneously preserved ONL cell counts (Figure 4H) and ONL thickness (Figure 4I). The remaining TUNEL-positive apoptotic photoreceptors showed AIF translocation into the nucleus in *fog/fog* mice (Figure 4, C and F). Ultrastructural studies showed that, in contrast to RD-treated WT retinas, *fog/fog* retinas contained well-preserved rod spherules and cone pedicles in the outer plexiform layer (Figure 4, J and M, arrowheads), decreased apoptotic nuclei in the ONL (Figure 4, K and N, arrows), and relatively well preserved mitochondria in the inner segment of the photoreceptors (Figure 4, L and O, white arrows). Together, these results suggest that Apaf-1–dependent caspase activation contributes to RD-triggered photoreceptor neurodegeneration.

A cell-permeable peptide corresponding to the BH4 domain of Bcl-X$_L$ inhibits photoreceptor apoptosis. The above-mentioned data indicate that (at least) 2 postmitochondrial cell death pathways participate in RD-induced photoreceptor apoptosis, namely AIF (which mediated caspase-independent apoptosis) and Apaf-1 (which mediated cytochrome *c*–dependent caspase activation in the apoptosome). Both AIF and the apoptosome are activated as a result of MOMP.

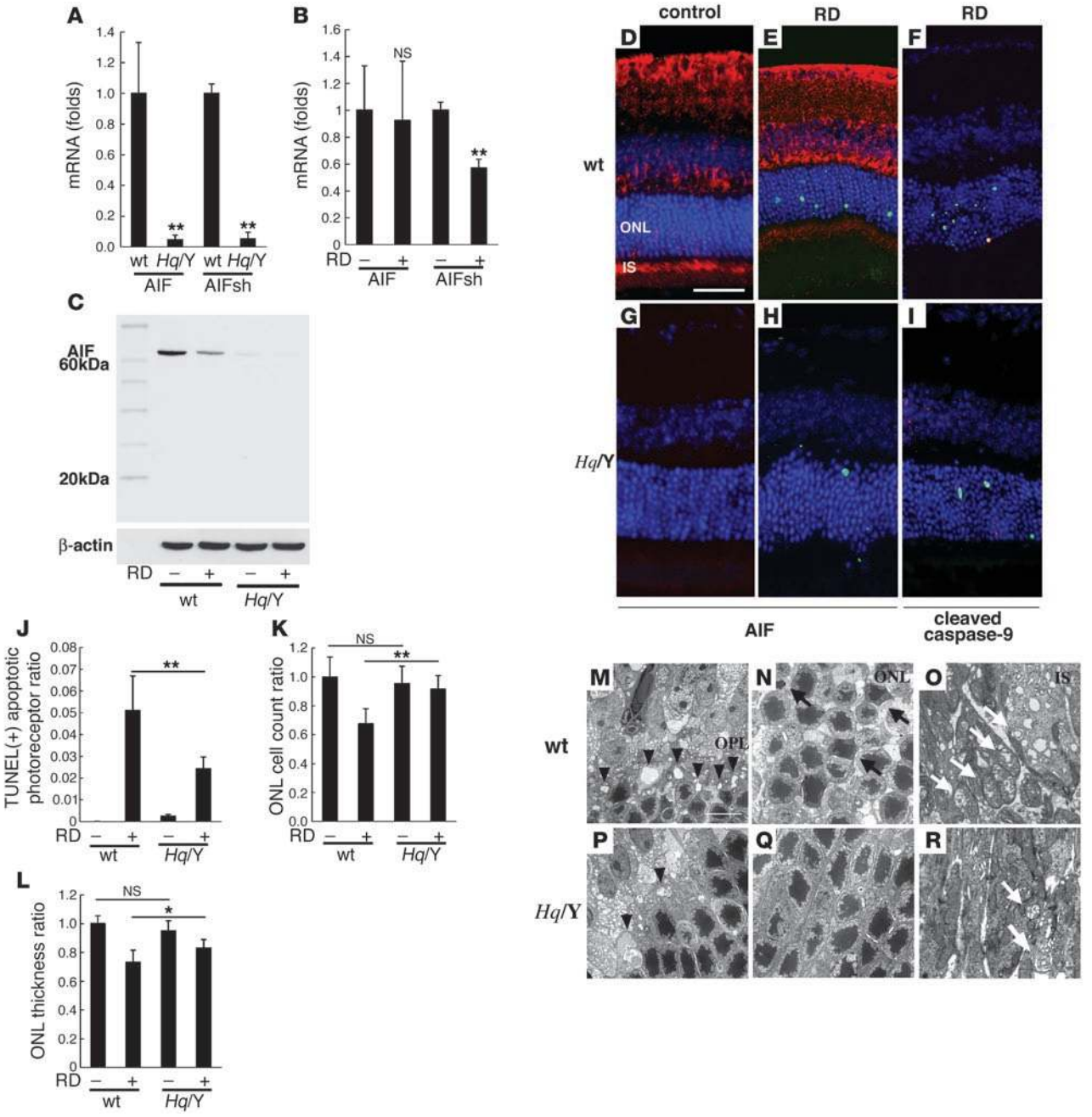

Figure 3

AIF deficiency protects from RD-induced photoreceptor apoptosis. To examine the AIF expression in retinas of AIF mutant mice (*Hq*/Y), we compared the expression of AIF and AIFsh mRNA (**A** and **B**) and AIF protein (**C**) in WT and *Hq*/Y mice before and after RD. *Hq*/Y mice exhibited negligible levels of AIF mRNA or AIF protein in contrast to WT mice (**A**–**C**). We also examined the expression of AIFsh, a proapoptotic short variant of AIF. The AIFsh mRNA expression was also decreased in AIF-deficient mice (*Hq*/Y*;* **A** and **B**), and AIFsh protein expression was not induced by RD in WT or *Hq*/Y mice (**C**). AIF immunohistochemistry confirmed the low AIF expression in *Hq*/Y mice (**G** and **H**; AIF in red, TUNEL in green, DAPI in blue) in contrast to WT mice (**D** and **E**). AIF deficiency in *Hq*/Y mice substantially decreased TUNEL-positive apoptotic cells after RD (**E**, **H**, and **J**) and preserved ONL cell count (**K**) and ONL thickness (**L**). The remaining TUNEL-positive apoptotic photoreceptors showed activated, cleaved caspase-9 in *Hq*/Y mice (**F** and **I**, caspase-9 in red). Electron microscopy also showed well-preserved rod spherules and cone pedicles in the outer plexiform layer (**M** and **P**, arrowheads; degenerated pedicles and spherules), decreased apoptotic nuclei in the ONL (**N** and **Q**, arrows), and relatively preserved mitochondria in the inner segment of photoreceptors (**O** and **R**, white arrows). $n = 5$ per group; $^{*}P < 0.05$, $^{**}P < 0.01$. Scale bars: 50 μm (**D**), 10 μm (**M**).

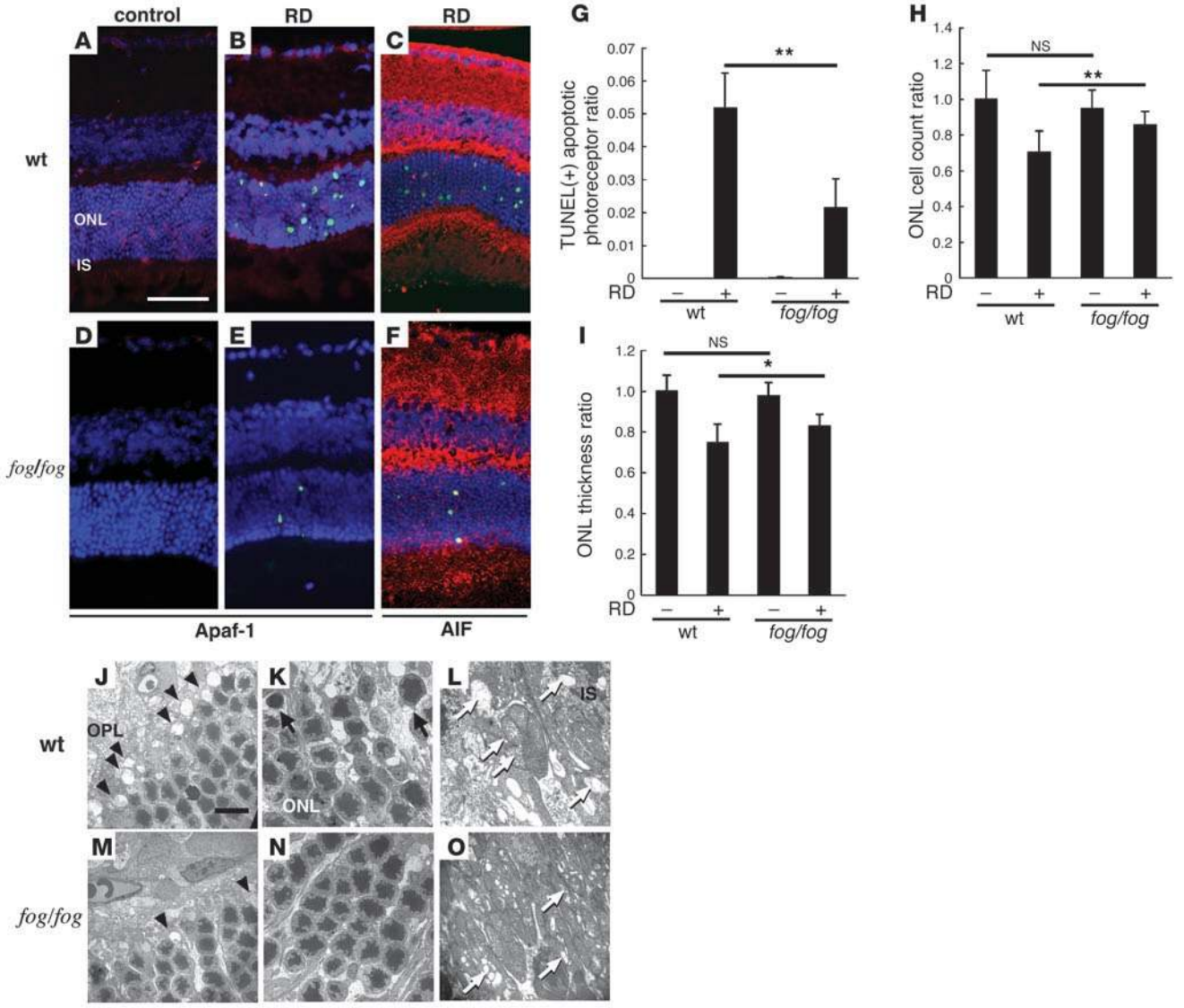

Figure 4

Apaf-1 deficiency protects from RD-induced photoreceptor apoptosis. Apaf-1 expression was observed in WT mice (**A** and **B**; Apaf-1 in red, TUNEL in green, DAPI in blue) but deficient in Apaf-1 mutant *fog/fog* mice (**D** and **E**). TUNEL-positive apoptotic photoreceptor after RD decreased in *fog/fog* mice in contrast to WT mice (**A**–**G**). The remaining TUNEL-positive apoptotic photoreceptors showed AIF translocation into the nucleus in *fog/fog* mice (**C** and **F**; AIF in red, TUNEL in green, DAPI in blue). In *fog/fog* mice, ONL cell count ratio (**H**) and ONL thickness ratio (**I**) were also preserved, in contrast to those in WT mice. Ultrastructural studies showed relatively well-preserved structures in the outer plexiform layer (**J** and **M**, arrowheads; rod spherules and cone pedicles), the ONL (**K** and **N**, arrows; apoptotic photoreceptors), and the inner segment of photoreceptors (**L** and **O**, white arrows; ruptured mitochondria). $n = 5$ per group; $^{*}P < 0.05$, $^{**}P < 0.01$. Scale bars: 50 μm (**A**), 10 μm (**J**).

We therefore investigated whether direct inhibition of MOMP might reduce RD-induced photoreceptor loss using a cell-permeable MOMP-inhibitory recombinant fusion protein, HIV-TAT BH4, composed of the HIV-TAT plasma membrane translocation domain and the antiapoptotic Bcl-X_L–derived BH4 domain. Intraperitoneal injection of HIV-TAT protein led to its distribution into photoreceptor cells, as this was seen after addition of HIV-TAT BH4 to primary retinal cell cultures (in vitro) (Supplemental Figure 1; supplemental material available online with this article; doi:10.1172/JCI34267DS1). The protective effect of HIV-TAT BH4 protein on the mitochondrial transmembrane potential was confirmed in primary retinal cell cultures (Supplemental Figure 2). Intraperitoneal injections of HIV-TAT BH4 reduced the frequency of RD-induced TUNEL-positive apoptotic photoreceptors in a dose-dependent manner (Figure 5, A–E). Simultaneously, HIV-TAT BH4 injections (but not injections of vehicle or a HIV-TAT control peptide) reduced the RD-triggered AIF translocation from inner segment mitochondria into nuclei (Figure 5, B and F) as well as caspase-9 cleavage (Figure 5, D and F). These findings underscore the likely importance of MOMP for RD-induced photoreceptor apoptosis.

Oral administration of HIV PIs prevents RD-induced photoreceptor apoptosis in vivo. Mice receiving a combination of oral nelfinavir (NFV) and ritonavir (RIT) that allowed for the maintenance of sustained

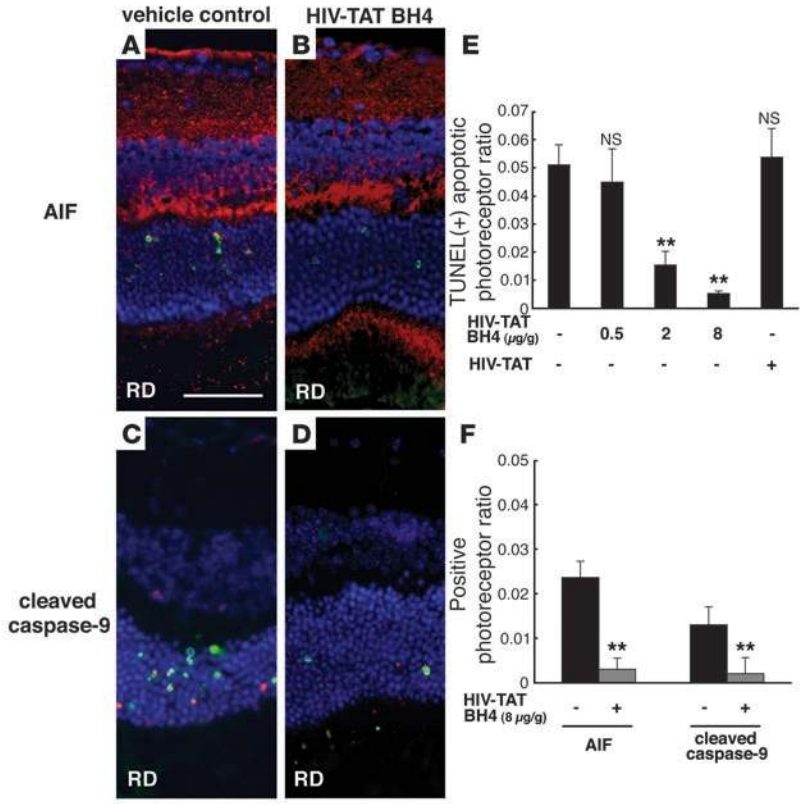

Figure 5
Intraperitoneal injection of recombinant Bcl-X_L fusion protein (HIV-TAT BH4) containing cell-permeable TAT protein transduction domain and antiapoptotic domain BH4 of Bcl-X_L attenuated apoptotic photoreceptors after RD in a dose-dependent manner. Notably, HIV-TAT BH4 protein also confined AIF translocation into the nucleus (**A**, **B**, and **F**; AIF in red, TUNEL in green, DAPI in blue) and decreased caspase-9 cleavage (**C**, **D**, and **F**; cleaved caspase-9 in red, TUNEL in green, DAPI in blue) after RD. Treatment of the animals with vehicle or a control cell-permeable HIV-TAT recombinant protein without the BH4 sequence did not affect photoreceptor apoptosis detected by TUNEL (**E**). $n = 5$ per group; $^{**}P < 0.01$. Scale bar in **A**: 50 μm.

NFV plasma levels were compared with sham-treated mice in their response to RD. NFV/RIT significantly decreased the frequency of RD-induced TUNEL-positive photoreceptors as well as AIF- and caspase-9–positive cells (Figure 6, A, B–E, and H). The ONL cell count ratio (Figure 6F) and ONL thickness ratio (Figure 6G) also confirmed that NFV/RIT counteracted the RD-triggered photoreceptor loss. Accordingly, the retinal ultrastructures were relatively well preserved in the NFV/RIT-treated cohort subjected to RD (Figure 6, L–N), as compared with the vehicle only–treated animals with RD (Figure 6, I–K). In the outer plexiform layer, where the photoreceptors and secondary neurons synapse, rod spherules and cone pedicles were well preserved in the NFV/RIT-treated group (Figure 6L), while they were degenerated in the vehicle-treated group (Figure 6I). In the ONL, photoreceptors with characteristics of apoptosis, such as cellular shrinkage and chromatin condensation, were also less frequent in the PI-treated group (Figure 6M) than in vehicle controls (Figure 6J). In the inner segment of the photoreceptors, a large number of mitochondria were found to swell in response to RD (Figure 6K), and this degenerative process was largely suppressed by treatment with NFV/RIT (Figure 6N). To examine whether PIs might mediate their photoreceptor-protective effects indirectly, via suppression of microglial activity, we quantified the microglial infiltration/proliferation in the retina after RD by immunofluorescence detection of the leukocyte common antigen CD45 (Figure 7, A, B, and E) and the macrophage/microglial marker CD11b (Figure 7, C, D, and F). Irrespective of the treatment with NFV/RIT, RD increased the frequency of $CD45^+$ cells or $CD11b^+$ cells in the outer plexiform layer (Figure 7, E and F). The number of infiltrating $CD45^+$ and $CD11b^+$ cells tended to decrease with the PI treatment. However, this difference did not reach significance. RD may cause infiltration of cells from the myeloid lineage, which may stimulate photoreceptor apoptosis (10), and conversely photoreceptor apoptosis may trigger infiltration of phagocytotic cells into the subretinal space (43). Our results suggest that the cytoprotective effects of PIs may not be subordinate to their putative antiinflammatory effects, but further studies will be needed to clarify this point.

Cytoprotective effects of the HIV PI NFV on photoreceptors in primary retinal cell cultures. To further investigate whether NFV is capable of exerting cell-autonomous apoptosis inhibition of photoreceptors, we investigated its effect on primary retinal cell cultures in which photoreceptor apoptosis was either induced by starvation (due to the withdrawal of the B27 supplement) or by coculture with primary macrophages from GFP-transgenic mice in the presence of the cytokine monocyte chemoattractant protein–1 (MCP-1; CCL2) (10). Retinal cell survival assessed by calcein AM decreased after starvation or upon coculture with macrophages, and this decrease was blunted by the addition of 7 μM NFV (Figure 8, A–E, and P). The number of $recoverin^+$ photoreceptors attaching on the culture dish decreased after 24 hours of starvation or coculture with macrophages by approximately two-thirds (Figure 8, F–J, and Q). This decline was again reduced by addition of NFV (Figure 8, F–J, and Q). Similar data were obtained when cell survival was assessed by an alternative method, namely staining of the cells with the mitochondrial transmembrane potential–sensitive dye MitoTracker CMTMRos. After starvation or macrophage stimulation, the frequency of retinal cells with intact mitochondria (red fluorescence) was strongly reduced, and this effect was antagonized by NFV treatment (Figure 8, K–O and R). The cytoprotective effect of NFV decreased after 24 hours of culture but was still significant at 72 hours (Figure 8, P–R). Both starvation and coculture with macrophages induced photoreceptors to

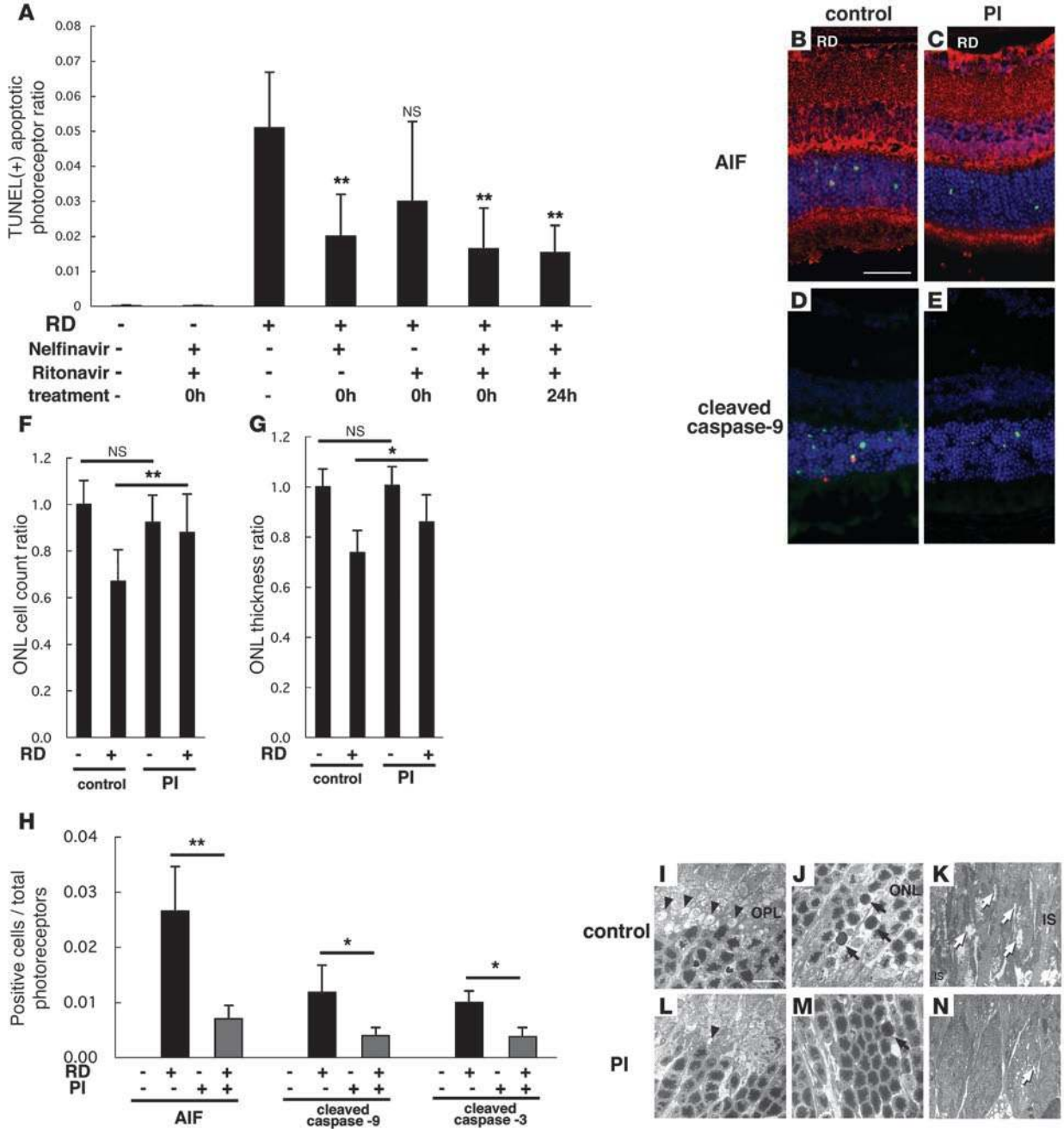

Figure 6

Systemic oral administration of HIV PIs prevents detachment-induced photoreceptor apoptosis as well as AIF translocation and caspase activation in vivo. Each animal received vehicle (2% ethanol in dH_20), single PI (NFV or RIT), or double PI (NFV boosted with RIT) 3 times daily, starting immediately after induction of RD (0h) or 24 hours after RD. Although NFV plus RIT did not affect control retina without RD, NFV and NFV/RIT substantially reduced TUNEL-positive apoptotic photoreceptors after RD (**A**–**E**). NFV/RIT also blocked AIF translocation from mitochondria to nuclei (**B**, **C**, and **H**; AIF in red, TUNEL in green, DAPI in blue) and caspase-9 and -3 cleavage (**D**, **E**, and **H**; cleaved caspase-9 in red, TUNEL in green, DAPI in blue). PIs preserved the ONL cell count ratio (**F**) and ONL thickness ratio (**G**). NFV/RIT also maintained the ultrastructure of the retinas after RD (**I**–**N**). In the outer plexiform layer (**I** and **L**), rod spherules and cone pedicles were well preserved in the NFV/RIT-treated group (**L**, arrowheads; degenerated pedicles and spherules) in contrast to the vehicle group (**I**). In the ONL, photoreceptors with characteristics of apoptosis (arrows), namely cellular shrinkage and chromatin condensation, decreased in the PI-treated group (**M**) in contrast to the vehicle-treated group (**J**). In the inner segment of photoreceptors, a large number of mitochondria was swollen and degenerated in the vehicle group (**K**, arrows); in contrast, mitochondria was well preserved in the PI-treated group (**N**). $n = 5$ per group; $^*P < 0.05$, $^{**}P < 0.01$. Scale bars: 50 μm (**B**), 10 μm (**I**).

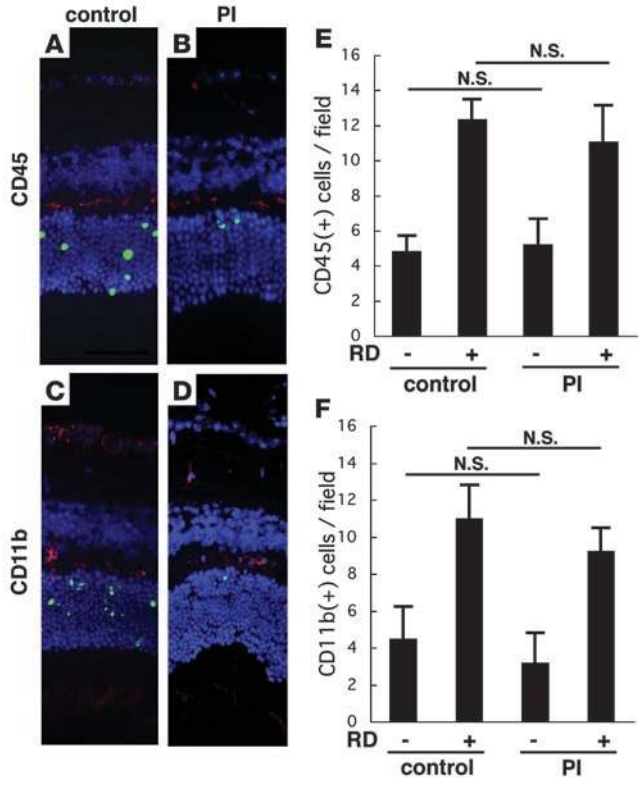

Figure 7
Accumulation of CD45+ and CD11b+ myeloid lineage cells in the retina after RD. To examine whether PIs might mediate their photoreceptor-protective effects indirectly, via suppression of microglial activity, we quantified the microglial infiltration/proliferation in the retina after RD by immunofluorescence detection of the leukocyte common antigen CD45 (**A**, **B**, and **E**; CD45 in red, TUNEL in green, DAPI in blue) and the macrophage/microglial marker CD11b (**C**, **D**, and **F**; CD11b in red, TUNEL in green, DAPI in blue) in control RD (**A** and **C**) and NFV/RIT-treated RD mice (**B** and **D**). Irrespective of the treatment with NFV/RIT, RD increased the frequency of CD45+ cells or CD11b+ cells in the outer plexiform layer (**E** and **F**). $n = 5$ per group.

undergo DNA fragmentation with TUNEL positivity (Figure 9, D, J, and M), to translocate AIF from mitochondria into the nucleus (Figure 9, A, C, and M), and to activate caspase-9 in the cytoplasm (Figure 9, G, I, and M), as demonstrated by immunofluorescence microscopy. NFV treatment reduced all these manifestations of the mitochondrial cell death pathway (Figure 9, E, F, and K–M). To confirm the relocalization and activation of proapoptotic molecules, we performed subcellular fractionation experiments and purified cytosolic and mitochondrial proteins (Supplemental Figure 4). The capacity of NFV to inhibit the mitochondrial release of AIF and cytochrome *c*, as well as the activation of caspase-9, was corroborated by immunoblot analyses of the subcellular fractions (Figure 9N). Together, these results confirm the capacity of NFV to interrupt the apoptotic pathway by inhibiting MOMP, presumably by a direct action on photoreceptor cells.

Effect of HIV PIs on circulating CD4+CD8+ T cells. The number of $CD4^+CD8^+$ T cells in the blood was determined by flow cytometry (Supplemental Figure 5). The ratio of circulating $CD4^+$ to $CD8^+$ cells in the blood did not change significantly during the 3 days of the experimental period with PI administration. Thus, the neuroprotective action of PIs did not correlate with effects on peripheral T cells.

Discussion

In this work, we demonstrate, for the first time to our knowledge, that HIV PIs inhibit the mitochondrial release of AIF in addition to suppressing the translocation of cytochrome *c*. Thus, HIV PIs interrupt both the caspase-dependent (cytochrome *c*/Apaf-1/caspase-9–mediated) and the caspase-independent (AIF-mediated) pathways of self-destruction that originate in the mitochondria. This may explain why PIs inhibit apoptotic cell death in clinically relevant models of neurodegeneration, while pharmacological caspase inhibition largely fails to protect neurons in vivo (6, 31, 44).

In this study, we showed AIF translocation into the nucleus and caspase-9 activation in the cytoplasm of TUNEL-positive photoreceptors from human specimens with RD, suggesting that both AIF and the mitochondrial pathway of caspase activation contribute to photoreceptor degeneration. Mice carrying a hypomorphic mutation of the *Aif* gene (*Hq*/Y) exhibited a significantly reduced photoreceptor apoptosis after RD. Embryonic stem cells with a targeted null mutation in AIF have previously been reported to resist apoptosis induction by serum starvation, underscoring the apoptogenic role of AIF (45) and supporting our results in vivo and in vitro from RD and retinal primary cell cultures with or without PIs. We took advantage of another mouse strain carrying a hypomorphic mutation of *Apaf1* (*fog/fog*) to examine the role of the Apaf-1–dependent cytochrome *c*–mediated caspase activation cascade in RD. The Apaf-1 deficiency also reduced photoreceptor apoptosis. These results are in line with the reports on studies using $Apaf1^{-/-}$ mouse embryo fibroblasts that showed resistance against mitochondria-dependent apoptotic stimuli but not against the death receptor–mediated, mitochondria-independent pathway (40).

Neither *Hq*/Y nor *fog/fog* mice were completely protected against RD-induced photoreceptor apoptosis. There are two possibilities that may explain this phenomenon. One is that residual amounts of AIF and Apaf-1 allow some apoptosis to occur in these hypomorphic mutants. As an alternative (and nonexclusive) possibility, molecular interactions between the different pathways might compensate for each other during the apoptotic process. AIF induces purified mitochondria to release cytochrome *c* and caspase-9, suggesting that AIF, once released from mitochondria, accelerates membrane permeabilization in a positive feed-forward loop (16). While released cytochrome *c* binds Apaf-1 that in turn activates caspase-9, caspases can also directly affect mitochondrial function and/or disrupt mitochondrial membrane permeability (46). We hypothesize that both pathways are activated after MOMP and simultaneously orchestrate complementary pathways culminating in cellular demise in the neurodegenerative model of RD. This hypothesis is supported by the fact that antiapoptotic HIV-TAT BH4 protein, which inhibits MOMP and hence blocks the release of both cytochrome *c* and AIF (47, 48), successfully reduced photoreceptor apoptosis after RD. Furthermore, administration of HIV-TAT BH4 protein had additive protective effects on the *Hq*/Y mouse, where it decreased the activation of caspase-9.

The fine mechanisms of the antiapoptotic action of PIs remain elusive. We examined whether PIs block the accumulation of inflammatory cells in the retina to contribute the neuroprotec-

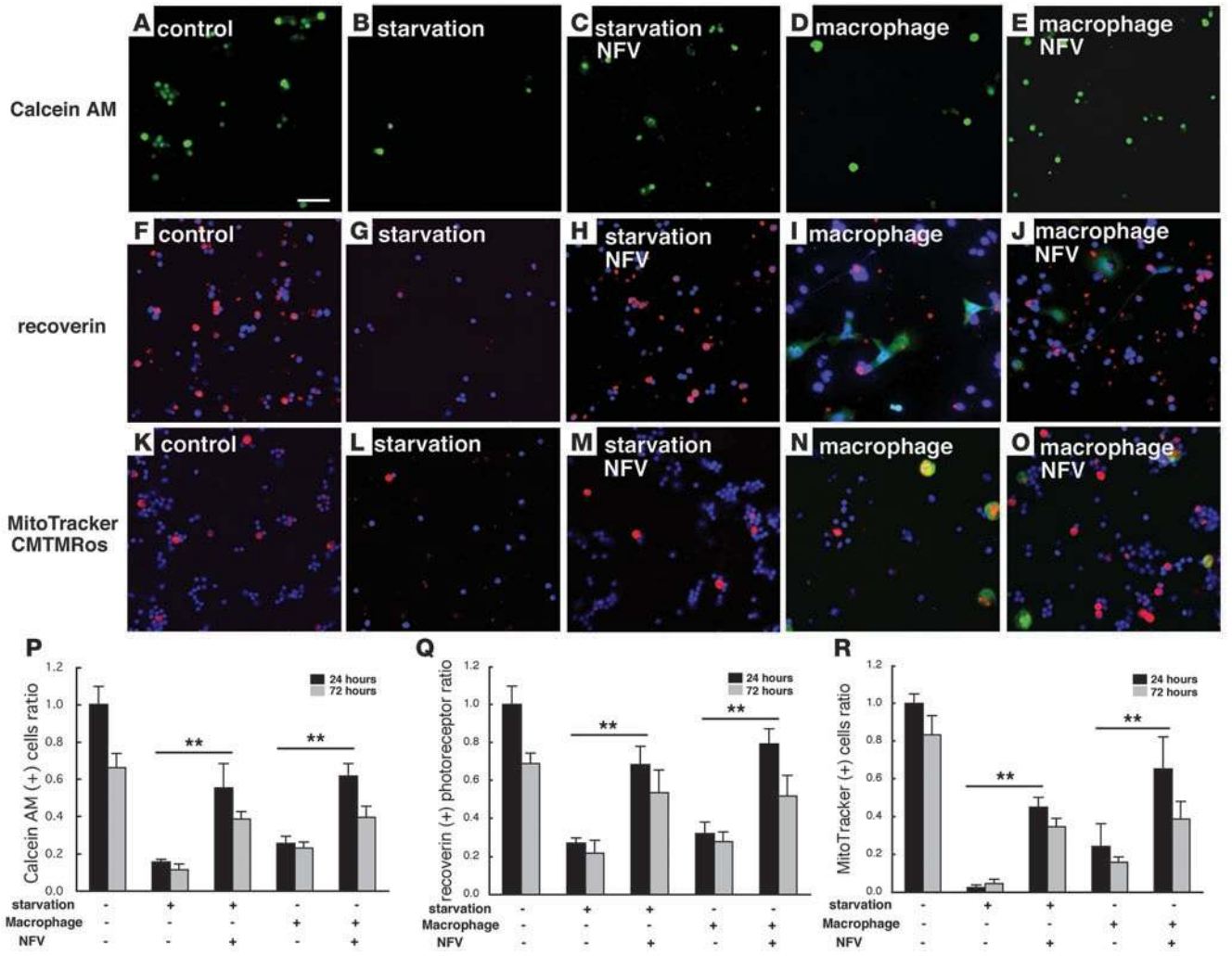

Figure 8

PI increased survival of photoreceptors and preserved mitochondrial potential in vitro in 2 models of primary retinal cell cultures. The viability of retinal cells was measured with calcein AM after starvation or after coculture with macrophages (**A**–**E** and **P**; calcein AM in green). Calcein-positive viable cells decreased after starvation (**B**) or coculture (**D**) as compared with untreated control (**A**). PI (NFV, 7 μM) treatment significantly increased calcein-positive cells (**C** and **E**). Recoverin$^+$ photoreceptors attaching on culture dish were analyzed after starvation or coculture with macrophages (**F**–**J** and **Q**; recoverin in red, GFP in green, DAPI in blue). Attaching recoverin$^+$ photoreceptors decreased after 24 hours incubation (**G** and **I**) as compared with untreated control cultures (**F**). PI treatment significantly rescued photoreceptors from apoptotic cell death (**H** and **J**). Mitochondrial function was assessed by a mitochondrial potential–sensitive dye, CMTMRos. CMTMRos intake (**K**–**O**, **R**; CMTMRos in red, GFP in green, DAPI in blue) was lost after induction of apoptosis (**L** and **N**) but reversed in NFV-treated cells (**M** and **O**). Representative images are shown (**A**–**O**), and the quantified results are shown in **P**–**R**. n = 10 per group; $^{**}P < 0.01$. Scale bar: 100 μm.

tive effect. Although PIs were reported to have direct effects on CD4$^+$CD8$^+$ T cells and leukocytes (24), we failed to observe any effects of PIs on the frequency of circulating inflammatory cells during the 3-day treatment period (Supplemental Figure 5). Furthermore, PIs failed to significantly reduce the accumulation of CD45$^+$ or CD11b$^+$ cells in the retina following RD. These results may suggest that PIs block the proapoptotic consequences of the inflammatory cell accumulation (10) rather than inflammation itself. In photoreceptors, PIs decreased the mitochondrio-nuclear AIF translocation, as well as the activation of caspase-9 and -3, resulting in decreased apoptotic photoreceptor cell loss. Comparable results were obtained both in vivo and in primary retinal cell cultures, indicating that PIs can exert their neuroprotective effects without the need of metabolic modifications in the general circulation, through a direct effect on the stressed cell type. Interestingly, when PIs are used at concentrations higher than therapeutic concentrations, they exert a proapoptotic effect under certain conditions, mostly in tumor models (49, 50). High concentrations of PIs (10–50 μM, about 1 magnitude above the therapeutic level) inhibit proliferation and induce apoptosis in murine and human cell lines (49), adult T cell leukemia (ATL) cells (51), and multiple myeloma cells (52), correlating with a cell-cycle arrest in G_1 phase (49) and decreased expression of anti-apoptotic proteins (51, 52). It is unclear how PIs induce apoptosis at high concentrations, and further studies will be needed to elucidate their full clinical potentials.

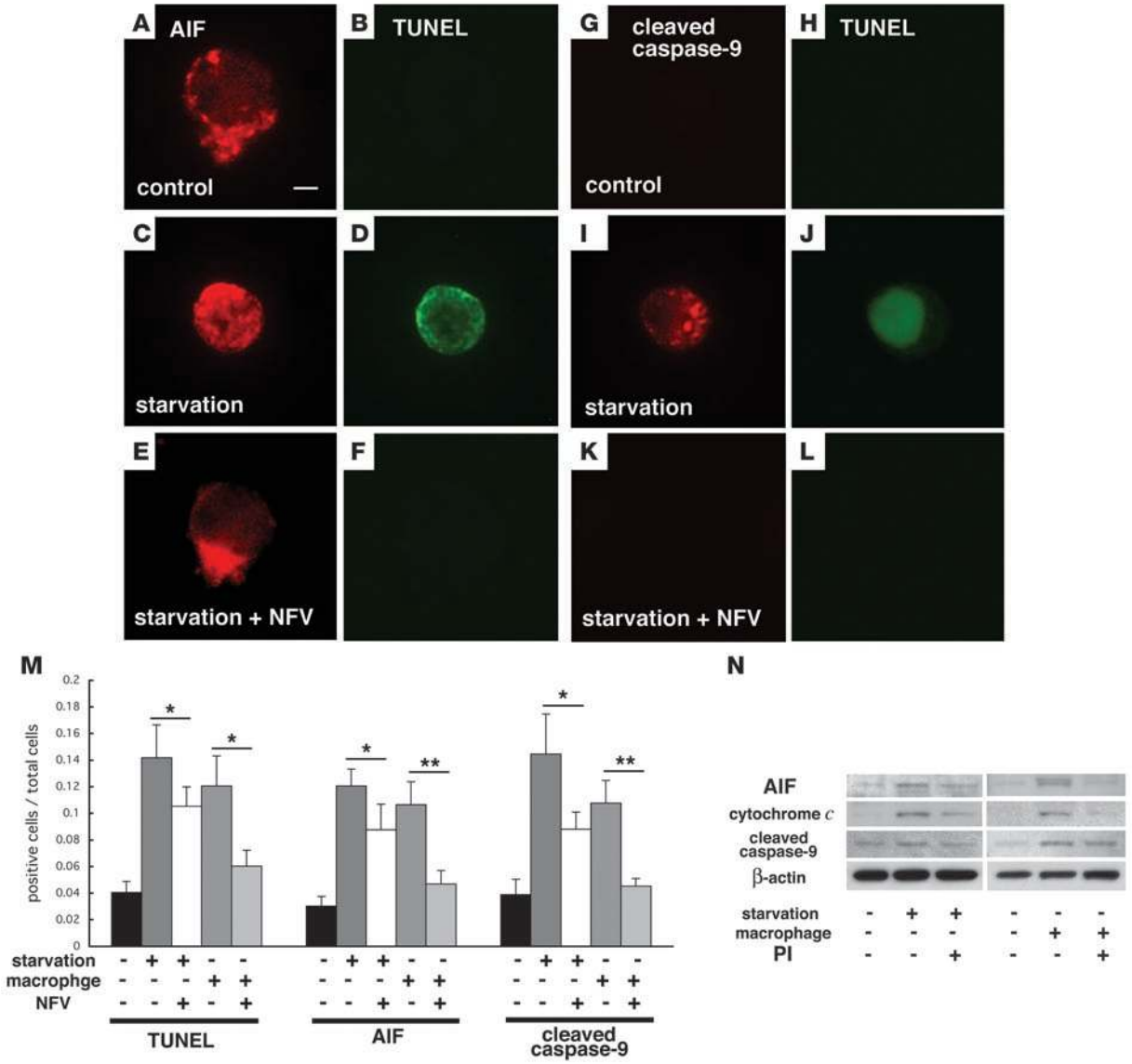

Figure 9

PI blocked leakage of proapoptotic molecules from the mitochondria to the cytosol (AIF and cytochrome *c*) and subsequent activation of caspase-9 in vitro. Representative images of immunofluorescence detection of AIF (**A**–**F**; AIF in red, TUNEL in green) and cleaved activated caspase-9 (**G**–**L**; cleaved caspase-9 in red, TUNEL in green) in control photoreceptor cultures (**A**, **B**, **G**, and **H**) and after starvation in the absence (**C**, **D**, **I**, and **J**) or presence of NFV (**E**, **F**, **K**, and **L**). Photoreceptors underwent TUNEL-detectable apoptosis in starvation and macrophage coculture models but were preserved by treatment with NFV (**M**). AIF translocation and caspase-9 cleavage were also decreased by NFV treatment (**M**). Immunoblot analyses of cytosolic fractions showed AIF and cytochrome *c* translocation from the mitochondria to the cytosol and subsequent caspase-9 cleavage under starvation or macrophage cocultures, and these changes were suppressed by NFV treatment (**N**). $n = 10$ per group; $^{*}P < 0.05$, $^{**}P < 0.01$. Scale bar in **A**: 1 μm.

It is noteworthy that, in the mouse model of RD, the antiapoptotic effects of PIs were observed in a setting in which PIs are administered *after* the apoptosis-initiating event. Based on this observation and based on the well-known low toxicity of acute PI administration, we believe that the administration of PIs should be clinically evaluated, especially during the interval between diagnosed (or suspected) RD and reattachment surgery. Photoreceptor degeneration, which is the ultimate cause of vision loss, occurs acutely after the detachment and may continue chronically if reattachment is not complete. Administration of a drug capable of preventing photoreceptor loss would be highly useful between the onset of RD and reattachment surgery. In the present study, we demonstrated that PIs (administered orally 3 times daily) blocked the mitochondrial release of critical proapoptotic proteins such as AIF and cytochrome *c* and reduced photoreceptor apoptosis. Taken together with our in vitro data and those of a previous report (34), these results indicate that PIs stabilized MOMP by presumably binding the adenine nucleotide translocator. The blockade of photoreceptor apoptosis correlated with preserved cell counts and ONL thickness, which are major indicators

of preserved retinal function. Thus, although PIs cannot reattach the retina, they might be clinically useful for preventing critical visual loss during RD and hence increase the chance of therapeutic success. Moreover, there are many retinal disorders related to RD, such as diabetic retinopathy or age-related macular degeneration, that cause abnormal vascular permeability or neovascularization. In addition to these ophthalmic applications, PIs might be considered for the treatment or prevention of other mitochondrion-triggered neurodegenerative processes.

Methods

AIF translocation and caspase activation in human retina after RD. All human materials were used under a protocol approved by the human studies committee for research-related use of human material of the Massachusetts Eye and Ear Infirmary (MEEI) and in accordance with the Declaration of Helsinki. Ten normal eyes and 4 RD eyes were selected based on pathology reports in the archives of the David G. Cogan Eye Pathology Laboratory at MEEI. The normal retina and RD were noted macroscopically prior to embedding and confirmed microscopically. We examined H&E-stained sections of the selected specimens to confirm the characteristic features of RD, such as separation of the retina from the RPE and degeneration of the photoreceptor outer segment. These RD specimens were then examined by immunohistochemistry for AIF and cleaved caspase-9 and compared with control specimens. Representative images are shown in Figure 1. The RD eyes were an autopsy specimen from a 65-year-old patient with hypertension who died from an intracerebral hemorrhage and an eye bank specimen from a 51-year-old patient who died from massive coronary thrombosis. The control eye was an autopsy specimen from a 61-year-old patient with hypertension who died from a cerebrovascular accident.

Experimental animals. All animal procedures were performed in accordance with the statement of the Association for Research in Vision and Ophthalmology and a protocol approved by the Animal Care Committee of MEEI. GFP-transgenic mice (C57BL/6-Tg[UBC-GFP]30Scha/J; stock number 004353) with uniform GFP expression controlled by the human ubiquitin C promoter were purchased from The Jackson Laboratory. Adult (8 weeks of age) male mice were used for the following experiments.

Surgical induction of RD. Mouse experimental RD was induced by a previously described method (6). Briefly, the mice were anesthetized with an intraperitoneal injection of pentobarbital, and their pupils were dilated with topical 1% tropicamide and 2.5% phenylephrine hydrochloride. The retinas were detached using a subretinal injection of 1% sodium hyaluronate (Healon; Pharmacia). Sodium hyaluronate was gently injected through the sclera into the subretinal space to enlarge the RDs. RD was induced only in the right eye of each animal, and 5 eyes were examined in each group. The mice were sacrificed 3 days after treatment, and their eyes were harvested for the following studies.

RD-induced photoreceptor apoptosis in AIF-deficient mice. We used *Hq* mice to examine the role of AIF in photoreceptor apoptosis after RD. We examined the mRNA and protein expression of AIF and AIFsh, a proapoptotic short variant that is reported to be induced after apoptotic insults (22), by RT-PCR and Western blot analysis, respectively, in hemizygote (*Hq*/Y) and WT (+/Y) mice. Then we induced RD in *Hq* and WT mice, and the eyes were harvested for immunohistochemistry, Western blotting, and electron microscopy. RD was created only in the right eye of each animal, and 5 eyes were examined in each group. The tissue samples were assigned numbers and letters, and the conditions were masked from the observers. The 5 sections were randomly selected in each eye, and the central area of the detached retina was analyzed by ImageJ software (http://rsb.info.nih.gov/ij/) on immunohistochemistry, TUNEL analysis, and determination of ONL thickness and ONL column cell count. The results are presented as mean ± SD.

RD-induced photoreceptor apoptosis in Apaf-1–deficient mice. We used *fog/fog* mice to examine the role of Apaf-1 and Apaf-1–dependent cytochrome *c*–mediated apoptotic cascade in photoreceptor apoptosis after RD.

The heterozygote (*fog/fog*) mice and WT (+/+) mice underwent surgical induction of RD, and the eyes were harvested for immunohistochemical analysis and electron microscopy. RD was induced only in the right eye of each animal, and 5 eyes were examined in each group. The 5 sections were randomly selected in each eye, and central area of the detached retina was analyzed by ImageJ software.

Blockade by BH4 domain peptide from Bcl-X_L fused to the transduction domain of HIV-TAT protein (HIV-TAT BH4). Cell-penetrating peptide constructs such as HIV-1 TAT basic domain and related peptides have been developed to deliver bioactive peptides into cells (47, 48, 53–58). Rapid and receptor-independent uptake of TAT-conjugated peptides have been demonstrated to occur in vitro and in vivo (54). We tested whether systemic delivery of recombinant Bcl-X_L fusion protein (HIV-TAT BH4) containing TAT protein transduction domain attenuates photoreceptor apoptosis after RD in vivo and in primary retinal culture in vitro. The mice received intraperitoneal injection of vehicle (PBS), HIV-TAT BH4 (0.5, 2, 8 μg/g BW; Calbiochem; EMD), and HIV-TAT control peptide (8 μg/g BW; Calbiochem) without BH4 sequence followed by induction of RD. RD was induced only in the right eye of each animal, and 5 eyes were examined in each group. The eyes were harvested on day 3 and analyzed by immunohistochemistry and TUNEL. For primary retinal cell culture, the retinal cells were incubated with HIV-TAT BH4 (1 μM) for 24 hours.

Inhibition of apoptosis by systemic oral administration of HIV PIs. We evaluated the impact of the HIV PIs NFV, RIT, and NFV boosted with RIT in models of nonviral disease, i.e., RD associated with pathological apoptosis. As mouse metabolism of PI differs from that of humans, we first performed pharmacokinetic study of mice to provide a level of NFV similar to that found in human therapy (34). The mice received oral administration of 125 mg/kg BW NFV and/or 13 mg/kg RIT 3 times daily following induction of RD. The drug dosing that we used results in therapeutic levels of NFV, in the range of 3–5 μM, and undetectable levels of RIT. The K_i of NFV for the HIV protease enzyme is about 2 nM. Control animals received vehicle (2% ethanol) 3 times daily after RD. RD was induced only in the right eye of each animal, and 5 eyes were examined in each group. The eyes were harvested 3 days after RD and PI treatment. Results of immunohistochemical analysis and electron microscopy as well as ONL cell count and thickness ratios are shown.

TUNEL. TUNEL analysis and quantification of TUNEL-positive cells were performed as previously described (6) using the ApopTag Fluorescein In Situ Apoptosis Detection Kit (Chemicon International; Millipore). The center of the detached retina was photographed, and the TUNEL-positive cells in the ONL were counted in a masked fashion. The results are presented as mean ± SD.

Immunohistochemistry. Immunohistochemistry was performed as previously reported (6). Rabbit anti-AIF (R&D Systems), anti-mouse cleaved caspase-3 and -9 (Cell Signaling Technology), anti-recoverin (Chemicon International; Millipore), anti–Apaf-1 (Sigma-Aldrich), rat anti-mouse CD45 (BD Biosciences — Pharmingen), and anti-mouse CD11b (BD Biosciences — Pharmingen) were used as primary antibodies and incubated at 4°C overnight. A nonimmune serum was used as a negative control. Alexa Fluor 546–conjugated goat anti-rabbit IgG (Invitrogen), Cy5-conjugated anti rat IgG (Zymed; Invitrogen), and anti-rabbit IgG (Zymed; Invitrogen) were used as secondary antibodies and incubated at room temperature for 1 hour.

Transmission electron microscopy. The eyes were enucleated, and the posterior segments were fixed in 2.5% glutaraldehyde and 2% paraformaldehyde in 0.1 M cacodylate buffer with 0.08 M $CaCl_2$ at 4°C. The detached reti-

nas were removed and post-fixed for 1.5 hours in 2% aqueous OsO_4, dehydrated in ethanol and water, and embedded in EPON. Ultrathin sections were cut from blocks and stained with saturated, aqueous uranyl acetate and Sato's lead stain. The specimens were observed with a Philips CM10 electron microscope.

Adult mouse primary retinal cultures. Adult primary retinal cultures were prepared as previously described with minor modifications (10). Neural retinas were incubated at 37°C for 20 minutes in a CO_2 incubator in digestion solution containing papain (10 U/ml; Worthington Biochemical Corp.) and L-cysteine (0.3 mg/ml; Sigma-Aldrich) in HBSS. Cell density was adjusted to 3.5×10^4 cells for each well of an 8-well chamber (Nunc) with Neurobasal-A medium (Invitrogen) containing B27 supplement without antioxidants (NBA/B27AO$^-$; Invitrogen) and 1 μg/ml insulin, 2 mM L-glutamate, and 12 μg/ml gentamicin. We performed immunocytochemistry with a rabbit anti-recoverin antibody (Chemicon International; Millipore) to determine the number of attaching photoreceptor cells in the culture. For starvation, cells were cultured in Neurobasal-A medium without B27 supplement and incubated for 3 hours (Western blotting) and 24 hours (immunohistochemistry). For macrophage stimulation, an immunopanning dish was prepared by incubating culture dishes (10 cm; Falcon) with rat anti-CD11b antibody (50 μg/ml; Serotec) in 4 ml HBSS overnight. The panning dish was blocked with 4 ml HBSS/0.1% BSA for 1 hour, and dissociated cells were incubated in the dish for 30 minutes, with slow agitation of the dish every 10 minutes. For determination of CD11b$^+$ cells, macrophages were collected from GFP-transgenic mice as previously described (10, 59) and added to retinal primary culture after depletion of residual macrophages/microglia (10). One hour later, MCP-1 (1 ng/ml) was added to the culture medium, and incubation continued for 3 hours (Western blotting) and 24 hours (immunohistochemistry). For PI treatment, the cultures were cocultured with 7 μM NFV in the medium in both starvation and macrophage stimulation. The recoverin$^+$ cells were counted in 10 random fields per well in a masked fashion using ImageJ software. Values are given as mean ± SEM of 10 replicate wells.

Viability assay by intracellular esterase activity in primary retinal cell cultures. To assess the viability of primary retinal cells, we used calcein AM (Invitrogen). Intracellular esterases convert nonfluorescent calcein AM into intensely fluorescent calcein, which is only retained in live cells. For starvation, the cultures were incubated in Neurobasal medium without B27 for 24 hours and then exposed to 2 μM calcein AM for 45 minutes. For macrophage stimulation, the cultures were incubated for 24 hours with MCP-1 and then exposed to 2 μM calcein AM for 45 minutes. The cultures were covered with coverslips and observed by fluorescence microscopy. The calcein AM–positive cells were counted in 10 random fields per well in a masked fashion using ImageJ software. Values are given as mean ± SEM of 10 replicate wells.

Functional respiratory mitochondria staining by a derivative of tetramethylrosamine. To examine whether PIs also block the functional integrity of mitochondria, we added a derivative of tetramethylrosamine, MitoTracker Orange CMTMRos (M7510; Invitrogen), into the primary retinal cell cultures. The MitoTracker Orange CMTMRos probe passively diffuses across the plasma membranes and accumulates in active mitochondria, driven by the mitochondrial inner transmembrane potential (60, 61). For starvation, the cultures were incubated in Neurobasal medium without B27 for 24 hours and then exposed to 200 nM Orange CMTMRos for 45 minutes. For macrophage stimulation, the cultures were incubated for 24 hours with MCP-1 application and then exposed to 200 nM Orange CMTMRos for 45 minutes. The cultures were fixed with 4% paraformaldehyde and observed under a fluorescence microscope. CMTMRos-positive cells were counted in 10 random fields per well in a masked fashion using ImageJ software. Values are given as mean ± SEM of 10 replicate wells.

RNA extraction, reverse transcription, and real-time PCR. The expression levels of AIF and splice variant AIFsh in retinal tissues of WT and AIF mutant mice were examined by real-time PCR. In brief, the retinal tissues were obtained from 3 eyes of WT and AIF mutant mice under normal conditions and 3 days after RD and homogenized in extraction reagent (PureLink Total RNA Purification System; Invitrogen) according to the manufacturer's protocol. Equal amounts of extracted total RNA were reverse transcribed with a First-Strand cDNA Synthesis Kit (GE Healthcare) at 37°C for 1 hour in a 15-μl reaction volume. For semiquantitative analysis of AIF and AIFsh expression, a real-time PCR assay was performed with Prism 7700 Sequence Detection System (Applied Biosystems), according to the manufacturer's protocol. TaqMan Gene Expression assays (Applied Biosystems) were used to check the expression of AIF and AIFsh and GAPDH. Although these sequences of commercially available primers were undocumented, these primers were designed for spanning between exon 1 and exon 2 (AIF) and intron 9 and exon 10 (AIFsh), not to detect genomic fragments. The cycling conditions were 50°C for 2 minutes, initial denaturation at 95°C for 10 minutes, and 40 cycles at 95°C for 15 seconds and 60°C for 1 minute. The quantity of mRNA expression was calculated by normalizing the Ct value of AIF and AIFsh to the Ct of endogenous control GAPDH in the same sample, according to the comparative $\Delta\Delta C_T$ method (10, 62). Each experiment was performed at least twice, and representative data are shown.

Protein extraction, cellular fractionation, and Western blot analysis. For protein extraction, proteins from retinas of WT and AIF-deficient mice were harvested using Mammalian Cell Lysis Kit (Sigma-Aldrich) according to the manufacturer's protocol. For cellular fractionation, the cytosolic and mitochondrial fractions were collected from primary retinal cell culture using Mitochondrial Fractionation Kit (Active Motif) according to the manufacturer's protocol.

For Western blot analysis, 20 μg of the cell extracts were resolved by 10% SDS-PAGE under reducing conditions and transferred onto polyvinylidene difluoride membranes (Invitrogen). The membranes were incubated with StartingBlock Blocking Buffer (Pierce Biotechnology) to block nonspecific reaction and then exposed to the rabbit anti-AIF antibody (R&D Systems) overnight at 4°C. After the membranes were washed 3 times with PBS containing 2% Tween-20 (Sigma-Aldrich), they were incubated with peroxidase-conjugated anti-rabbit IgG (GE Healthcare). Chemiluminescence reagents (ECL Western Blot Analysis Detection Reagents; GE Healthcare) were used to visualize the labeled protein bands according to the manufacturer's instructions. The membranes were then incubated with stripping buffer (Restore Buffer; Pierce Biotechnology) and examined with cytochrome *c* (BD Biosciences — Pharmingen), cleaved caspase-9 (Cell Signaling Technology), Tim23 (BD Biosciences), and β-actin antibodies (Sigma-Aldrich), respectively. Each experiment was performed at least twice, and representative data are shown.

Flow cytometry for CD4$^+$CD8$^+$ T cells in circulating blood with/without HIV PIs. As PIs were originally reported to increase the number of CD4$^+$ T cells after HIV infection (24) as well as CD8$^+$ cells (63) and leukocytes (25), we examined leukocyte characteristics by flow cytometry to determine whether the neuroprotective effect of PIs depends on the number of CD4$^+$CD8$^+$ T cells. To analyze the phenotype of circulating leukocytes in the blood, leukocytes were collected from 3 control mice and 3 mice 3 days after RD with or without systemic oral administration of PIs (NFV boosted with RIT). Whole blood was collected, and the leukocytes were adjusted to the designated concentrations. The cells were incubated with IgG for blocking nonspecific FcR, followed by rat anti-mouse CD4-FITC/CD8-PE or isotype control–FITC/PE (AbD Serotec), respectively. Flow cytometry was performed with EPICS XL (Beckman Coulter). The number of circulating CD4$^+$CD8$^+$ T cells was calculated from the percent of each population. The

gate of $CD4^+CD8^+$ T cells was set up according to the staining pattern of isotype control (IgG-FITC/PE).

Statistics. The statistical significance of RT-PCR results was determined using unpaired 2-tailed *t* tests. The data from the TUNEL and in vitro survival assays were analyzed with the Scheffé post-hoc test using StatView 4.11J software for Macintosh (Abacus Concepts Inc.). Significance level was set at $P < 0.05$ (*) and $P < 0.01$ (**). The data represent mean ± SD, except for the primary culture results, for which data represent mean ± SEM.

Acknowledgments

We thank Mari Imamura and Fumiyo Morikawa (Kyushu University) and Kennard Thomas and Sreedevi Mallemadugula (MEEI) for technical assistance. This work was supported by an Alcon Research Award (to J.W. Miller), the Japan Eye Bank Association (to T. Hisatomi), a Bausch & Lomb Vitreoretinal Fellowship (to T. Nakazawa), NIH grant AI50775 (to A. Hafezi-Moghadam), National Eye Institute grant EY014104 (MEEI Core Grant), Agence Nationale pour la Recherche (to G. Kroemer), the NIH (R01 AI62261 and R01 AI403840 to A.D. Badley), and the Burroughs Wellcome Fund's Clinical Scientist Award in Translational Research (ID no. 1005160 to A.D. Badley). We would like to thank the Massachusetts Lions Eye Research Fund for generous funds provided for laboratory equipment used in this project and Research to Prevent Blindness for unrestricted funds awarded to the Department of Ophthalmology at Harvard Medical School.

Received for publication October 18, 2007, and accepted in revised form April 2, 2008.

Address correspondence to: Joan W. Miller, Massachusetts Eye and Ear Infirmary, 243 Charles Street, Boston, Massachusetts 02114, USA. Phone: (617) 573-3526; Fax: (617) 573-3364; E-mail: joan_miller@meei.harvard.edu. Or to: Guido Kroemer, INSERM U848, Institut Gustave Roussy, Pavillon de Recherche 1, F-94805 Villejuif (Paris), France. Phone: 33-1-42-11-60-46; Fax: 33-1-42-11-60-47; E-mail: kroemer@igr.fr.

1. Dunaief, J.L., Dentchev, T., Ying, G.S., and Milam, A.H. 2002. The role of apoptosis in age-related macular degeneration. *Arch. Ophthalmol.* **120**:1435–1442.
2. Barber, A.J., et al. 1998. Neural apoptosis in the retina during experimental and human diabetes. Early onset and effect of insulin. *J. Clin. Invest.* **102**:783–791.
3. Fulton, A.B., Hansen, R.M., Petersen, R.A., and Vanderveen, D.K. 2001. The rod photoreceptors in retinopathy of prematurity: an electroretinographic study. *Arch. Ophthalmol.* **119**:499–505.
4. Cook, B., Lewis, G.P., Fisher, S.K., and Adler, R. 1995. Apoptotic photoreceptor degeneration in experimental retinal detachment. *Invest. Ophthalmol. Vis. Sci.* **36**:990–996.
5. Berglin, L., Algvere, P.V., and Seregard, S. 1997. Photoreceptor decay over time and apoptosis in experimental retinal detachment. *Graefes Arch. Clin. Exp. Ophthalmol.* **235**:306–312.
6. Hisatomi, T., et al. 2001. Relocalization of apoptosis-inducing factor in photoreceptor apoptosis induced by retinal detachment in vivo. *Am. J. Pathol.* **158**:1271–1278.
7. Zacks, D.N., et al. 2003. Caspase activation in an experimental model of retinal detachment. *Invest. Ophthalmol. Vis. Sci.* **44**:1262–1267.
8. Arroyo, J.G., Yang, L., Bula, D., and Chen, D.F. 2005. Photoreceptor apoptosis in human retinal detachment. *Am. J. Ophthalmol.* **139**:605–610.
9. Nakazawa, T., et al. 2006. Characterization of cytokine responses to retinal detachment in rats. *Mol Vis* **12**:867–878.
10. Nakazawa, T., et al. 2007. Monocyte chemoattractant protein 1 mediates retinal detachment-induced photoreceptor apoptosis. *Proc. Natl. Acad. Sci. U. S. A.* **104**:2425–2430.
11. Green, D.R., and Kroemer, G. 2004. The pathophysiology of mitochondrial cell death. *Science.* **305**:626–629.
12. Bao, Q., Riedl, S.J., and Shi, Y. 2005. Structure of Apaf-1 in the auto-inhibited form: a critical role for ADP. *Cell Cycle.* **4**:1001–1003.
13. Bao, Q., and Shi, Y. 2007. Apoptosome: a platform for the activation of initiator caspases. *Cell Death Differ.* **14**:56–65.
14. Acehan, D., et al. 2002. Three-dimensional structure of the apoptosome: implications for assembly, procaspase-9 binding, and activation. *Mol. Cell.* **9**:423–432.
15. Bouchier-Hayes, L., Lartigue, L., and Newmeyer, D.D. 2005. Mitochondria: pharmacological manipulation of cell death. *J. Clin. Invest.* **115**:2640–2647.
16. Susin, S.A., et al. 1999. Molecular characterization of mitochondrial apoptosis-inducing factor. *Nature.* **397**:441–446.
17. Cande, C., et al. 2004. AIF and cyclophilin A cooperate in apoptosis-associated chromatinolysis. *Oncogene.* **23**:1514–1521.
18. Wang, H., Shimoji, M., Yu, S.W., Dawson, T.M., and Dawson, V.L. 2003. Apoptosis inducing factor and PARP-mediated injury in the MPTP mouse model of Parkinson's disease. *Ann. N. Y. Acad. Sci.* **991**:132–139.
19. Chu, C.T., Zhu, J.H., Cao, G., Signore, A., Wang, S., and Chen, J. 2005. Apoptosis inducing factor mediates caspase-independent 1-methyl-4-phenylpyridinium toxicity in dopaminergic cells. *J. Neurochem.* **94**:1685–1695.
20. Sanges, D., Comitato, A., Tammaro, R., and Marigo, V. 2006. Apoptosis in retinal degeneration involves cross-talk between apoptosis-inducing factor (AIF) and caspase-12 and is blocked by calpain inhibitors. *Proc. Natl. Acad. Sci. U. S. A.* **103**:17366–17371.
21. Loeffler, M., et al. 2001. Dominant cell death induction by extramitochondrially targeted apoptosis-inducing factor. *FASEB J.* **15**:758–767.
22. Delettre, C., et al. 2006. AIFsh, a novel apoptosis-inducing factor (AIF) pro-apoptotic isoform with potential pathological relevance in human cancer. *J. Biol. Chem.* **281**:6413–6427.
23. Green, D.R., and Kroemer, G. 2005. Pharmacological manipulation of cell death: clinical applications in sight? *J. Clin. Invest.* **115**:2610–2617.
24. Staszewski, S., et al. 1999. Efavirenz plus zidovudine and lamivudine, efavirenz plus indinavir, and indinavir plus zidovudine and lamivudine in the treatment of HIV-1 infection in adults. Study 006 Team. *N. Engl. J. Med.* **341**:1865–1873.
25. Phenix, B.N., Cooper, C., Owen, C., and Badley, A.D. 2002. Modulation of apoptosis by HIV protease inhibitors. *Apoptosis.* **7**:295–312.
26. Deeks, S.G., and Grant, R.M. 1999. Sustained CD4 responses after virological failure of protease inhibitor-containing therapy. *Antivir. Ther.* **4**:7–11.
27. Badley, A.D. 2005. In vitro and in vivo effects of HIV protease inhibitors on apoptosis. *Cell Death Differ.* **12**:924–931.
28. Estaquier, J., et al. 2002. Effects of antiretroviral drugs on human immunodeficiency virus type 1-induced CD4(+) T-cell death. *J. Virol.* **76**:5966–5973.
29. Sloand, E.M., et al. 1999. Human immunodeficiency virus type 1 protease inhibitor modulates activation of peripheral blood CD4(+) T cells and decreases their susceptibility to apoptosis in vitro and in vivo. *Blood.* **94**:1021–1027.
30. Ghibelli, L., et al. 2003. Anti-apoptotic effect of HIV protease inhibitors via direct inhibition of calpain. *Biochem. Pharmacol.* **66**:1505–1512.
31. Phenix, B.N., Lum, J.J., Nie, Z., Sanchez-Dardon, J., and Badley, A.D. 2001. Antiapoptotic mechanism of HIV protease inhibitors: preventing mitochondrial transmembrane potential loss. *Blood.* **98**:1078–1085.
32. Matarrese, P., et al. 2003. Mitochondrial membrane hyperpolarization hijacks activated T lymphocytes toward the apoptotic-prone phenotype: homeostatic mechanisms of HIV protease inhibitors. *J. Immunol.* **170**:6006–6015.
33. Weaver, J.G., Rouse, M.S., Steckelberg, J.M., and Badley, A.D. 2004. Improved survival in experimental sepsis with an orally administered inhibitor of apoptosis. *FASEB J.* **18**:1185–1191.
34. Weaver, J.G., et al. 2005. Inhibition of adenine nucleotide translocator pore function and protection against apoptosis in vivo by an HIV protease inhibitor. *J. Clin. Invest.* **115**:1828–1838.
35. Barber, B.R. 1971. Research news. *Mouse News Lett.* **45**:34–35.
36. Klein, J.A., et al. 2002. The harlequin mouse mutation downregulates apoptosis-inducing factor. *Nature.* **419**:367–374.
37. Joza, N., et al. 2005. Muscle-specific loss of apoptosis-inducing factor leads to mitochondrial dysfunction, skeletal muscle atrophy, and dilated cardiomyopathy. *Mol. Cell. Biol.* **25**:10261–10272.
38. Harris, B.S., et al. 1997. Forebrain overgrowth (fog): a new mutation in the mouse affecting neural tube development. *Teratology.* **55**:231–240.
39. Honarpour, N., Gilbert, S.L., Lahn, B.T., Wang, X., and Herz, J. 2001. Apaf-1 deficiency and neural tube closure defects are found in fog mice. *Proc. Natl. Acad. Sci. U. S. A.* **98**:9683–9687.
40. Yoshida, H., et al. 1998. Apaf1 is required for mitochondrial pathways of apoptosis and brain development. *Cell.* **94**:739–750.
41. Cecconi, F., Alvarez-Bolado, G., Meyer, B.I., Roth, K.A., and Gruss, P. 1998. Apaf1 (CED-4 homolog) regulates programmed cell death in mammalian development. *Cell.* **94**:727–737.
42. Cecconi, F., and Gruss, P. 2001. Apaf1 in developmental apoptosis and cancer: how many ways to die? *Cell. Mol. Life Sci.* **58**:1688–1697.
43. Hisatomi, T., et al. 2003. Clearance of apoptotic photoreceptors: elimination of apoptotic debris into the subretinal space and macrophage-mediated phagocytosis via phosphatidylserine receptor and integrin alphavbeta3. *Am. J. Pathol.* **162**:1869–1879.
44. Hisatomi, T., et al. 2002. Critical role of Photoreceptor Apoptosis in Functional Damage after Retinal Detachment. *Curr. Eye Res.* **24**:161–172.
45. Joza, N., et al. 2001. Essential role of the mitochon-

drial apoptosis-inducing factor in programmed cell death. *Nature.* **410**:549–554.
46. Susin, S.A., et al. 1997. The central executioner of apoptosis: multiple connections between protease activation and mitochondria in Fas/APO-1/CD95- and ceramide- induced apoptosis. *J. Exp. Med.* **186**:25–37.
47. Shimizu, S., Konishi, A., Kodama, T., and Tsujimoto, Y. 2000. BH4 domain of antiapoptotic Bcl-2 family members closes voltage-dependent anion channel and inhibits apoptotic mitochondrial changes and cell death. *Proc. Natl. Acad. Sci. U. S. A.* **97**:3100–3105.
48. Cao, G., et al. 2002. In vivo delivery of a Bcl-xL fusion protein containing the TAT protein transduction domain protects against ischemic brain injury and neuronal apoptosis. *J. Neurosci.* **22**:5423–5431.
49. Gaedicke, S., et al. 2002. Antitumor effect of the human immunodeficiency virus protease inhibitor ritonavir: induction of tumor-cell apoptosis associated with perturbation of proteasomal proteolysis. *Cancer Res.* **62**:6901–6908.
50. Vlahakis, S.R., Bennett, S.A., Whitehead, S.N., and Badley, A.D. 2007. HIV protease inhibitors modulate apoptosis signaling in vitro and in vivo. *Apoptosis.* **12**:969–977.
51. Dewan, M.Z., Uchihara, J.N., Terashima, K., Honda, M., Sata, T., Ito, M., Fujii, N., Uozumi, K., Tsukasaki, K., Tomonaga, M., et al. 2006. Efficient intervention of growth and infiltration of primary adult T-cell leukemia cells by an HIV protease inhibitor, ritonavir. *Blood.* **107**:716–724.
52. Ikezoe, T., et al. 2004. HIV-1 protease inhibitor induces growth arrest and apoptosis of human multiple myeloma cells via inactivation of signal transducer and activator of transcription 3 and extracellular signal-regulated kinase 1/2. *Mol. Cancer Ther.* **3**:473–479.
53. Schwarze, S.R., Ho, A., Vocero-Akbani, A., and Dowdy, S.F. 1999. In vivo protein transduction: delivery of a biologically active protein into the mouse. *Science.* **285**:1569–1572.
54. Dietz, G.P., Kilic, E., and Bahr, M. 2002. Inhibition of neuronal apoptosis in vitro and in vivo using TAT-mediated protein transduction. *Mol. Cell. Neurosci.* **21**:29–37.
55. Asoh, S., et al. 2002. Protection against ischemic brain injury by protein therapeutics. *Proc. Natl. Acad. Sci. U. S. A.* **99**:17107–17112.
56. Sugioka, R., et al. 2003. BH4-domain peptide from Bcl-xL exerts anti-apoptotic activity in vivo. *Oncogene.* **22**:8432–8440.
57. Yin, W., et al. 2006. TAT-mediated delivery of Bcl-xL protein is neuroprotective against neonatal hypoxic-ischemic brain injury via inhibition of caspases and AIF. *Neurobiol. Dis.* **21**:358–371.
58. Hotchkiss, R.S., et al. 2006. TAT-BH4 and TAT-Bcl-xL peptides protect against sepsis-induced lymphocyte apoptosis in vivo. *J. Immunol.* **176**:5471–5477.
59. Maruyama, K., et al. 2005. Inflammation-induced lymphangiogenesis in the cornea arises from CD11b-positive macrophages. *J. Clin. Invest.* **115**:2363–2372.
60. Poot, M., et al. 1996. Analysis of mitochondrial morphology and function with novel fixable fluorescent stains. *J. Histochem. Cytochem.* **44**:1363–1372.
61. Keij, J.F., Bell-Prince, C., and Steinkamp, J.A. 2000. Staining of mitochondrial membranes with 10-nonyl acridine orange, MitoFluor Green, and MitoTracker Green is affected by mitochondrial membrane potential altering drugs. *Cytometry.* **39**:203–210.
62. Wilhelm, J., and Pingoud, A. 2003. Real-time polymerase chain reaction. *Chembiochem.* **4**:1120–1128.
63. Carr, A., Emery, S., Kelleher, A., Law, M., and Cooper, D.A. 1996. CD8+ lymphocyte responses to antiretroviral therapy of HIV infection. *J. Acquir. Immune Defic. Syndr. Hum. Retrovirol.* **13**:320–326.